Biophysical Journal (2018) **114**(5): 1204-1215
https://www.cell.com/biophysj/fulltext/S0006-3495(18)30145-0

Extension of Rapid Buffering Approximation to Ca^{2+} buffers with two binding sites

Victor Matveev

Department of Mathematical Sciences
New Jersey Institute of Technology
Newark, NJ 07102

matveev@njit.edu

Abstract

Fundamental cell processes such as synaptic neurotransmitter release, endocrine hormone secretion and myocyte contraction are controlled by highly localized calcium (Ca^{2+}) signals resulting from brief openings of trans-membrane Ca^{2+} channels. On short temporal and spatial scales, the corresponding local Ca^{2+} nanodomains formed in the vicinity of a single or several open Ca^{2+} channels can be effectively approximated by quasi-stationary solutions. The Rapid Buffering Approximation (RBA) is one of the most powerful of such approximations, and is based on the assumption of instantaneous equilibration of the bimolecular Ca^{2+} buffering reaction, combined with the conservation condition for the total Ca^{2+} and buffer molecule numbers. Previously, RBA has been generalized to an arbitrary arrangement of Ca^{2+} channels on a flat membrane, in the presence of any number of simple Ca^{2+} buffers with one-to-one Ca^{2+} binding stoichiometry. However, many biological buffers have multiple binding sites. For example, buffers and sensors phylogenetically related to calmodulin consist of two Ca^{2+}-binding domains (lobes), with each domain binding two Ca^{2+} ions in a cooperative manner. Here we consider an extension of RBA to such buffers with two inter-dependent Ca^{2+} binding sites. We show that in the presence of such buffers, RBA solution is given by the solution to a cubic equation, analogous to the quadratic equation describing RBA in the case of a simple, one-to-one Ca^{2+} buffer. We examine in detail the dependence of RBA accuracy on buffering parameters, in order to reveal conditions under which RBA provides sufficient precision.

Keywords: **calcium buffer, calcium nanodomain, cooperative buffer**

INTRODUCTION

Many fundamental physiological cell processes such as synaptic neurotransmitter release, hormone secretion and muscle contraction are controlled by highly localized Ca^{2+} signals triggered by the opening of a small number of trans-membrane Ca^{2+} channel (1-5). Intracellular Ca^{2+} buffers contribute to this tight localization of Ca^{2+} influx, absorbing most of the Ca^{2+} influx soon upon its entry into the cytoplasm (6, 7). Free Ca^{2+} ions remain localized in the vicinity of open Ca^{2+} channels, forming so-called Ca^{2+} *nanodomains*, while in the case of ryanodine and inositol 1,4,5-trisphosphate receptor-coupled Ca^{2+} channels, these local Ca^{2+} signals are referred to as *sparks* or *blinks* (5, 8, 9). It is a great challenge to image Ca^{2+} concentrations on fine spatio-temporal scales required to resolve these events, explaining the central role that mathematical and computational modeling of buffered Ca^{2+} diffusion has played in the study of Ca^{2+} dynamics in neurons, endocrine cells and myocytes (9-18).

One of the contributions of mathematical modeling was the development of accurate analytical approximations of quasi-stationary Ca^{2+} nanodomains (reviewed in (14, 19, 20)). Apart from providing insight into the dependence of Ca^{2+} concentration on the various buffering parameters, such approximations allow avoiding computationally expensive integration of reaction-diffusion equations or stochastic simulations, while retaining considerable accuracy (21-25). The most powerful of the previously developed approximations are the Rapid Buffering Approximation (RBA) (19, 23, 26-29) and the Linear Approximation (LIN) (14, 25, 30, 31). These two approximations have partially overlapping but distinct domains of applicability (19, 20), and can both be generalized to an arbitrary collection of buffers and any number of Ca^{2+} channels on a flat membrane. Further, RBA has the additional benefit of providing useful intuition about the non-equilibrium, time-dependent buffered Ca^{2+} diffusion problem (26-29). Several other approximations have also been considered (19, 20, 32, 33)

Despite their great utility, analytical approximations have only been developed for buffers with a single Ca^{2+} binding site, which we will refer to as simple, or one-to-one buffers. In contrast, most biological buffers possess several binding sites with distinct Ca^{2+} binding characteristics (Table 1). If the binding to such multiple sites are independent, they can be modeled as a combination of several simple buffers with binding properties that correspond to each of the distinct interaction sites, allowing the application of RBA or LIN. However, some widely expressed buffers and sensors like calretinin and calmodulin contain molecular domains that can bind two Ca^{2+} ions in a cooperative manner. This cooperativity in binding manifests itself in the higher affinity of the second Ca^{2+} ion binding compared to the first Ca^{2+} binding event (34, 35). This property is analogous to the cooperative binding of oxygen to hemoglobin. Most of the previously developed stationary nanodomain approximations cannot be straightforwardly extended to such realistic buffers. However, RBA can in fact be successfully generalized. Our goal is to analyze this extension of RBA to buffers composed of molecular domains with two Ca^{2+}-binding sites, which can be described with sufficient accuracy using mass-action description of the following reaction of a buffer molecule *B* (36):

$$B \underset{k_1^-}{\overset{2Cak_1^+}{\rightleftharpoons}} B^* \underset{2k_2^-}{\overset{Cak_2^+}{\rightleftharpoons}} B^{**} \qquad (1)$$

Here each asterisks represents Ca^{2+} ion bound to the buffer molecule. Denoting the affinities of the two reactions as $K_{1,2} = k_{1,2}^-/k_{1,2}^+$, the cooperativity in Ca^{2+} binding is quantified by the ratio $\varepsilon = K_2/K_1$. Thus, highly cooperative buffers are characterized by a small value of parameter ε (see Table 1). This condition interacts

in a non-trivial way with the small parameter quantifying the RBA assumption that reaction rate be much faster than the rate of Ca^{2+} influx and diffusion (19). Therefore, the range of applicability of RBA for cooperative buffers may be smaller than that for simple, non-cooperative buffers. Our goal is to systematically explore the parameter space to evaluate the accuracy of the RBA extension to two-to-one buffers, and show that in a certain parameter regime RBA retains sufficient accuracy. We hope that this contributes to the development of methods and tools for the modeling of realistic buffers, in view of the prominent role that cooperative buffer-sensors such as calmodulin play in a variety of fundamental physiological processes, including metabolism, apoptosis, myocyte contraction, intracellular motility, synaptic function, inflammation and immune response (34, 36-41).

MATERIALS AND METHODS

The following analysis follows earlier work on equilibrium solutions to buffered Ca^{2+} diffusion near point Ca^{2+} channel sources, reviewed in (19), but extends prior analysis to the case of complex buffers with two Ca^{2+} binding sites, as described by the biochemical reaction given by Eq. 1. We will denote B^* and B^{**} the partially and fully Ca^{2+}-bound states of the buffer (i.e. buffer molecule with a single or two bound Ca^{2+} ions, respectively). Denoting free [Ca^{2+}] as C, and time differentiation as ∂_t , one obtains the reaction-diffusion system

$$\begin{cases} \partial_t C = D_C \nabla^2 C - R_1 - R_2, \\ \partial_t B = D_B \nabla^2 B - R_1, \\ \partial_t B^* = D_B^* \nabla^2 B^* + R_1 - R_2, \\ \partial_t B^{**} = D_B^{**} \nabla^2 B^{**} + R_2. \end{cases} \tag{2}$$

The two reaction fluxes, R_1, R_2 are defined by applying the law of mass action to the reaction in Eq. 1:

$$\begin{cases} R_1 = 2k_1^+ C B - k_1^- B^*, \\ R_2 = k_2^+ C B^* - 2k_2^- B^{**}. \end{cases} \tag{3}$$

There are two independent linear combination of Eqs. 2 that cancel the reaction terms, yielding two conservation laws for the total buffer and the total Ca^{2+} concentrations, as in the case of a simple buffer (19, 20, 23, 42, 43)

$$\partial_t \left(B + B^* + B^{**} \right) = \nabla^2 \left(D_B B + D_B^* B^* + D_B^{**} B^{**} \right), \tag{4}$$

$$\partial_t \left(C + B^* + 2B^{**} \right) = \nabla^2 \left(D_C C + D_B^* B^* + 2D_B^{**} B^{**} \right). \tag{5}$$

These conservation laws can be used to eliminate two variables in Eqs. 2. Restricting our analysis to equilibrium solutions, we retain the following four equations for the four unknown concentrations:

$$\begin{cases} D_B \nabla^2 B = R_1, \\ D_B^{**} \nabla^2 B^{**} = -R_2, \\ \nabla^2 \left(D_B B + D_B^* B^* + D_B^{**} B^{**} \right) = 0, \\ \nabla^2 \left(D_C C + D_B^* B^* + 2D_B^{**} B^{**} \right) = 0. \end{cases} \tag{6}$$

Now, we consider a collection of channels with currents I_k^{Ca} at positions r_k (k=1,2,…,N) on an infinite flat membrane with zero [Ca^{2+}] at infinity (case of non-zero background [Ca^{2+}] is considered in the Appendix). We will assume Neumann (no flux) conditions for all concentrations at the membrane boundary, neglecting the

action of Ca^{2+} pumps and exchangers. In this case reflection symmetry can be used to extend the domain to the entire R^3 space. For a single channel, this domain has spherical symmetry with respect to the channel location, so the solution to Eqs. 6 depends only on the distance from the channel. Noting this, the two Laplace equations in Eqs. 6 are readily integrated, and the solution extended to the case of multiple channels using the superposition principle for the linear Laplace operator (19, 20, 23, 27):

$$D_B B + D_B^* B^* + D_B^{**} B^{**} = const = D_B B_T \tag{7}$$

$$D_C C + D_B^* B^* + 2D_B^{**} B^{**} = \frac{1}{2\pi z F} \sum_{k=1}^{N} \frac{I_k^{Ca}}{|r - r_k|} \tag{8}$$

Here z=2 is the valence of the Ca^{2+} ion, and F is the Faraday constant. The geometric factor in Eq. 8 equals 2π rather than 4π, because of the doubling of the volume by reflection symmetry. The integration constant on the right-hand side of Eq. 7 is determined by the value of this conserved linear combination of buffer concentrations infinitely far from the channel; our assumption of zero background $[Ca^{2+}]$ corresponds to the boundary condition $C_\infty = B_\infty^* = B_\infty^{**} = 0$, $B_\infty = B_T$, therefore $D_B B_\infty + D_B^* B_\infty^* + D_B^{**} B_\infty^{**} = D_B B_T$. If Ca^{2+} binding reduces buffer mobility ($D_B^* < D_B, D_B^{**} < D_B$), then Eq. 7 leads to an observation that $B+B^*+B^{**} > B_T$, reflecting a compensatory influx of buffers into the channel nanodomain. Therefore, in this case the total concentration of buffer is not uniform throughout the cell, and our parameter B_T should be interpreted as the total concentration of buffer far from the channel cluster: $B_T \equiv B_{T,\infty}$.

We note two critical simplifying assumptions implied by the adopted framework. First, our results are not applicable on spatial scales smaller than the pore radius, since the point-channel idealization and the infinite Ca^{2+} concentration at the channel location in Eq. 8 are clearly unphysical. In fact, Ca^{2+} concentration reaches a finite value at the channel pore of finite radius, and moreover, the dependence of Ca^{2+} current on the finite Ca^{2+} concentration gradient across the pore can be used to determine the amplitude of steady-state channel current (32, 44). Second, as noted above, the effect of Ca^{2+} pumps and exchangers is neglected, which will affect the accuracy of the approximation far from the channel. The contribution of linearized endoplasmic reticulum Ca^{2+} pumps to steady-state Ca^{2+} concentration approximation has been explored in (32).

Non-dimensionalization

We will non-dimensionalize Eqs. 6-8 similarly to the case of a simple buffer (19, 20), with a single Ca^{2+} channel of current I_{Ca} at the origin. Namely, we normalize Ca^{2+} and buffer concentrations by the affinity of the 2nd binding step and total buffer concentration, respectively:

$$c = \frac{C}{K_2},\ b = \frac{B}{B_T},\ b^* = \frac{B^*}{B_T},\ b^{**} = \frac{B^{**}}{B_T}. \tag{9}$$

We introduce dimensionless distance variable $\rho \equiv r / L$, where the length constant is given by

$$L = I_{Ca} / \left(4\pi F K_2 D_C\right). \tag{10}$$

This normalizes to unity the residue of the simple pole in $[Ca^{2+}]$ near the channel contributed by the point source: $\lim_{\rho \to 0} \rho c(\rho) = 1$, Then, Eqs. 6-8 read:

$$\begin{cases} \lambda\,\gamma\,\nabla_\rho^2 b \;=\; 2\varepsilon c\; b - b^*, \\ \lambda\;\delta_B^{**}\,\nabla_\rho^2 b^{**} = \; -c\; b^* + 2b^{**}, \\ b + \delta_B^* b^* + \delta_B^{**} b^{**} = 1, \\ c + \dfrac{\nu}{2}\left(\delta_B^* b^* + 2\delta_B^{**} b^{**}\right) = \dfrac{1}{\rho}. \end{cases} \tag{11}$$

where ∇_ρ^2 is the spherically symmetric Laplacian operator. The dimensionless quantities consist of parameters λ and ν analogous to the ones characterizing a simple, one-to-one buffer (see below and (19, 20)), plus parameters ε and γ characterizing cooperativity in Ca^{2+} binding, and two relative diffusivities δ_B^* and δ_B^{**} quantifying the effect of Ca^{2+} binding on buffer mobility:

$$\lambda = \frac{D_B}{L^2 k_2^-},\;\; \nu = \frac{2B_T D_B}{K_2\, D_C},\;\; \varepsilon = \frac{K_2}{K_1},\;\; \gamma = \frac{k_2^-}{k_1^-},\;\; \delta_B^* = \frac{D_B^*}{D_B},\;\; \delta_B^{**} = \frac{D_B^{**}}{D_B}. \tag{12}$$

Following prior work, in our numerical comparisons we will focus on the case where buffer mobility is not affected by Ca2+ binding: $\delta_B^{**} = \delta_B^* = 1$; however, for the sake of generality these parameters are included in all analytical expressions.

In Eqs. 11-12, λ is the dimensionless buffer mobility, analogous to ϵ_b in (19). It depends on both buffering parameters and Ca2+ current amplitude through length scale L (Eq. 10), and quantifies the ratio between the rate of diffusion on the one hand, and the rate of Ca2+ binding and influx on the other hand. Therefore, the Rapid Buffer Approximation (RBA) corresponds to $\lambda<<1$ (19). The accuracy of RBA may change with changing Ca2+ current, as explored in detail in (19) for the simple-buffer case.

Parameter ν quantifies the overall buffering strength, and equals the product of the relative buffer mobility, D_B / D_C (which we set to 0.1), and a quantity analogous to buffering capacity, $2B_T / K_2$. The concentration of binding sites for a two-site buffer equals $2B_T$, explaining the factor of 2. As the Ca^{2+} conservation condition in Eq. 11 shows, sufficiently close to the channel Ca2+ concentration is little perturbed from the free diffusion solution, $c=1/\rho$, unless ν is sufficiently large. In the notation adopted in (19), $\nu=1/\mu$.

The cooperativity in Ca2+ binding is quantified by the ratio of affinities of the two binding steps, $\varepsilon = K_2/K_1$. In the case of calretinin and calmodulin, the binding properties have been experimentally estimated, and the corresponding values of cooperativity parameters are given in Table 1 (cf. Table 4.2 in (19)). The value of parameter γ quantifies the degree to which binding cooperativity is caused by the slower 2nd unbinding step, as in C-lobe of calmodulin, as opposed to the faster 2nd Ca^{2+} binding, as in N-lobe of calmodulin.

Although the stoichiometric coefficients of 2 in Eqs. 11 and in the definition of ν could be removed by absorbing them into definitions of parameters K_1 and K_2 (see (39)), we choose to retain them for easier comparison to the case of a simple buffer. The previously obtained simple-buffer results corresponding to $\delta_B^{**} = \delta_B^* = \epsilon = \gamma = 1$ are thus easily recovered by substituting $\hat{b} = b + b^*/2,\; b^* = b^{**} + b^*/2$.

Numerical integration

To evaluate the accuracy of obtained RBA results, numerical integration of reaction-diffusion system given by Eqs. 2 is performed using the Calcium Calculator (CalC) modeling tool (45, 46) (Figs. 1-4). To ensure accuracy and convergence of these simulations, numerical grid size and equilibration time are automatically adjusted for each parameter combination using wrapper scripts written in MATLAB (Mathworks, Inc.)

Parameter	k_1^+ $(\mu M ms)^{-1}$	k_2^+ $(\mu M ms)^{-1}$	K_1 μM	K_2 μM	$\varepsilon = \frac{K_2}{K_1}$	$\gamma = \frac{k_2^-}{k_1^-}$	λ	ν
CaR coop. sites	0.0018	0.31	28	0.068	**$2.4 \cdot 10^{-3}$**	0.42	$1.6 \cdot 10^{-3}$	294
CaR non-coop.site	0.0073	--	36	--	--	--	--	
CaM N-lobe	0.77	32	193	0.788	**$4 \cdot 10^{-3}$**	0.17	$1.8 \cdot 10^{-4}$	25.4
CaM C-lobe	0.084	0.025	27.8	0.264	**$9.5 \cdot 10^{-3}$**	**$2.85 \cdot 10^{-3}$**	$7.8 \cdot 10^{-2}$	75.8

Table 1. Ca2+ binding properties of strongly cooperative buffers calretinin (CR) and calmodulin (CaM), as measured by Faas et al. (36, 40). Each CR molecule contains 5 binding sites, consisting of two identical cooperative pairs of Ca^{2+}-binding sites and one independent non-cooperative site. CaM molecule consists of two independent domains (lobes), each binding two Ca^{2+} ions in a cooperative manner. Note the very high rate of the 2nd Ca^{2+} binding rate to the N-lobe of CaM, which is therefore extremely diffusion-limited. Values of λ and ν are calculated for Ca^{2+} current strength of I_{Ca}=0.4 pA, and total buffer concentrations of B_T=100 μM.

RESULTS

Derivation of RBA

Rapid Buffer Approximation (RBA) is obtained by combining the conservation laws with the condition that reaction is at equilibrium. Therefore, we set R_1=R_2=0 in Eqs. 3, and use buffer conservation condition expressed by Eq. 7 to obtain

$$\begin{cases} B = \quad B_T K_1 K_2 \Big/ \left[K_1 K_2 + C(2\delta_B^* K_2 + \delta_B^{**} C) \right], \\ B^* = 2C B_T K_2 \Big/ \left[K_1 K_2 + C(2\delta_B^* K_2 + \delta_B^{**} C) \right], \\ B^{**} = \quad C^2 B_T \Big/ \left[K_1 K_2 + C(2\delta_B^* K_2 + \delta_B^{**} C) \right]. \end{cases} \tag{13}$$

For the case of invariant buffer mobility, $\delta_B^{**} = \delta_B^* = 1$, these expressions were first obtained in (39), but with stoichiometric factors of 2 absorbed in the definitions of the affinity parameters $K_{1,2}$, and expressed in terms of the reciprocals of these parameters.

Plugging these equilibrium conditions into the Ca^{2+} conservation Eq. 8 gives the RBA equation:

$$C\left[D_C + 2D_B B_T \frac{\delta_B^* K_2 + \delta_B^{**} C}{K_1 K_2 + C(2\delta_B^* K_2 + \delta_B^{**} \mathrm{C})} \right] = \frac{1}{4\pi F} \sum_{k=1}^{N} \frac{I_k^{Ca}}{|r - r_k|}. \tag{14}$$

This can be re-written as a cubic equation in C, with a single real positive root, obtainable in closed form (see below). The power of this approximation is that it is easy to extend to a set of M distinct two-site buffers with parameters $\left\{ B_{T,m}, D_{B,m}, \delta_m^*, \delta_m^{**}, K_{1,m}, K_{2,m} \right\}$, m=1..M:

$$C\left[D_C + 2\sum_{m=1}^{M} \frac{D_{B,m} B_{T,m} \left(\delta_m^* K_{2,m} + \delta_m^{**} C \right)}{K_{1,\mathrm{m}} K_{2,\mathrm{m}} + C\left(2\delta_m^* K_{2,\mathrm{m}} + \delta_m^{**} C \right)} \right] = \frac{1}{4\pi F} \sum_{k=1}^{N} \frac{I_k^{Ca}}{|r - r_k|}. \tag{15}$$

This equation can be converted to a polynomial equation in C of order $2M+1$, which is not solvable in closed form for $M > 1$. Still, numerical solution of this algebraic equation for each value of distance ρ presents a straightforward and computationally efficient algorithm of recovering nanodomain concentration approximation for any combination of cooperative buffers. Note that further generalizations are possible to any combination of buffers with arbitrary binding stoichiometry, beyond 2-to-1 binding considered in this study, by combining the full set of conservation conditions with the set of reaction equilibrium (detailed balance) conditions.

Nondimensional RBA

To systematically examine the accuracy of RBA, we will focus on the case of a single channel at the origin, and switch to non-dimensional variables, as outlined in Methods. This transforms the reaction equilibrium conditions in Eqs. 13 to the following simple form:

$$\begin{cases} b = 1\Big/\left[1+\varepsilon c\,(2\delta_B^{*}+\delta_B^{**}\,\mathrm{c})\right], \\ b^{*} = 2\varepsilon c\ \Big/\left[1+\varepsilon c\,(2\delta_B^{*}+\delta_B^{**}\,\mathrm{c})\right], \\ b^{**} = \varepsilon c^{2}\Big/\left[1+\varepsilon c\,(2\delta_B^{*}+\delta_B^{**}\,\mathrm{c})\right]. \end{cases} \tag{16}$$

The Rapid Buffer Approximation, Eq. 14, then becomes

$$c\left[1+\nu\varepsilon\frac{\delta_B^{*}+\delta_B^{**}c}{1+\varepsilon c\,(2\delta_B^{*}+\delta_B^{**}c)}\right]=\frac{1}{\rho}. \tag{17}$$

This equation is readily converted to a cubic equation in c, which has a single real positive root, corresponding to the closed-form expression for the RBA. It can be expressed in the form

$$c(\rho)=2V\cos\left(\frac{1}{3}\cos^{-1}\frac{U}{2V^{3}}\right)-F\,, \tag{18}$$

where functions F, A, V are determined by the algebraic system

$$\begin{cases} U = F\left(3G-2F^{2}\right)+\dfrac{1}{\delta_B^{**}\,\varepsilon\rho}, \\ V=\sqrt{F^{2}-G}, \\ F=\dfrac{1}{3}\left(\nu+\dfrac{2\delta_B^{*}}{\delta_B^{**}}-\dfrac{1}{\rho}\right), \\ G=\dfrac{1}{3\delta_B^{**}}\left(\delta_B^{*}\left(\nu-\dfrac{2}{\rho}\right)+\dfrac{1}{\varepsilon}\right). \end{cases} \tag{19}$$

Examination of the accuracy of RBA given by Eqs. 18-19 constitutes the main part of this study (see Figs. 1-4). To establish the connection of these results with the previously explored case of a simple buffer, consider two Ca^{2+} binding sites with identical affinities, and buffer mobility unaffected by Ca^{2+} binding, setting $\varepsilon=\delta_B^{*}=\delta_B^{**}=1$ in Eq. 17. Then one can extract a factor of (c+1) in the numerator and denominator of the 2nd term on the left-hand side of Eq. 17, reducing the equation order to quadratic. The resulting equation has one real positive root for any values of ρ and ν, corresponding to the simple-buffer RBA investigated previously (19). However, in the case where buffer mobility is affected by Ca^{2+} binding, there is no simple correspondence

between the two cases, and the corresponding RBA equation for the one-to-one buffer with variable diffusivity is modified to:

$$\left(c - 1/\rho\right)\left(1 + c\,\delta_B^*\right) + \nu\,\delta_B^*\,c = 0. \tag{20}$$

Accuracy of stationary RBA

We now turn to a systematic examination of the accuracy of the obtained stationary RBA approximation, using numerical simulations as a reference. As explored in detail by Smith et al. (19), simple-buffer RBA corresponds to an asymptotic singular perturbation expansion in parameter λ, for $\nu = O(1)$ (see also (20)). For moderate values of cooperativity parameters ($\varepsilon = O(1)$, $\gamma = O(1)$) one would expect the accuracy of the stationary RBA given by Eqs. Eqs. 18-19 to be similar to the accuracy of the RBA for the case of a simple (one-to-one) buffer. However, comparable accuracy is not at all guaranteed if the affinities of the two binding steps of a two-site buffer significantly differ, as in the case of cooperative buffers listed in Table 1. This is because cooperativity may manifest itself in the slow rate of the first of the two Ca^{2+} binding steps, while RBA requires that reaction rate be much faster than the rate of diffusion and Ca^{2+} influx. In other words, the parameter regime λ <<1 determining the RBA may have a complex interplay with the cooperativity condition ε <<1. Figure 1 illustrates this interplay between values of these nondimensional parameters in determining the accuracy of RBA. The values of λ and ν are fixed at λ=5·10^{-3} and ν=10, favoring RBA regime. Non-dimensional buffer concentrations *b, b** and *b*** are plotted on a linear scale in the first three rows of panels of Fig. 1, while *c*=[Ca^{2+}]/K_2 is shown on a logarithmic scale in the last row of panels, Fig. 1A4,B4,C4, since at small distances the source term dominates [Ca^{2+}].

When the two binding sites have equivalent properties (Fig. 1A1-A4), the agreement between RBA (*blue solid curves*) and numerical results (*dotted curves*) is excellent, as expected (19, 20). However, for ε = 0.1, the accuracy in buffer concentration estimation is significantly reduced (Fig. 1B1-B3), albeit the accuracy in [Ca^{2+}] approximation fares better (Fig. 1B4). Interestingly, we find that reducing γ along with ε partially rescues RBA accuracy (Fig. 1C1-C3). Thus, RBA is more accurate if buffer cooperativity is caused by the reduction of the unbinding rate of the second Ca^{2+} buffering reaction ($k_2^- \ll k_1^-$), as opposed to slow binding rate of the first buffering reaction ($k_2^+ >> k_1^+$). This result is intuitive, since RBA requires that Ca^{2+} binding rate be fast compared to the rate of diffusion. However, such intuitive interpretation should be treated with care since the value of RBA parameter λ depends on k_2^- as well. Parenthetically, we also note an interesting observation that the concentration of partially bound buffer, *b**, is a non-monotonic function of distance from the Ca^{2+} channel (Fig. 1A2,B2,C2), in contrast to the concentration of free and fully bound buffer. This property of a two-site buffer may potentially have physiological implications in terms of its downstream biochemical interactions, which are dependent on the conformational state of the buffer molecule, determined by the number of bound Ca^{2+} ions.

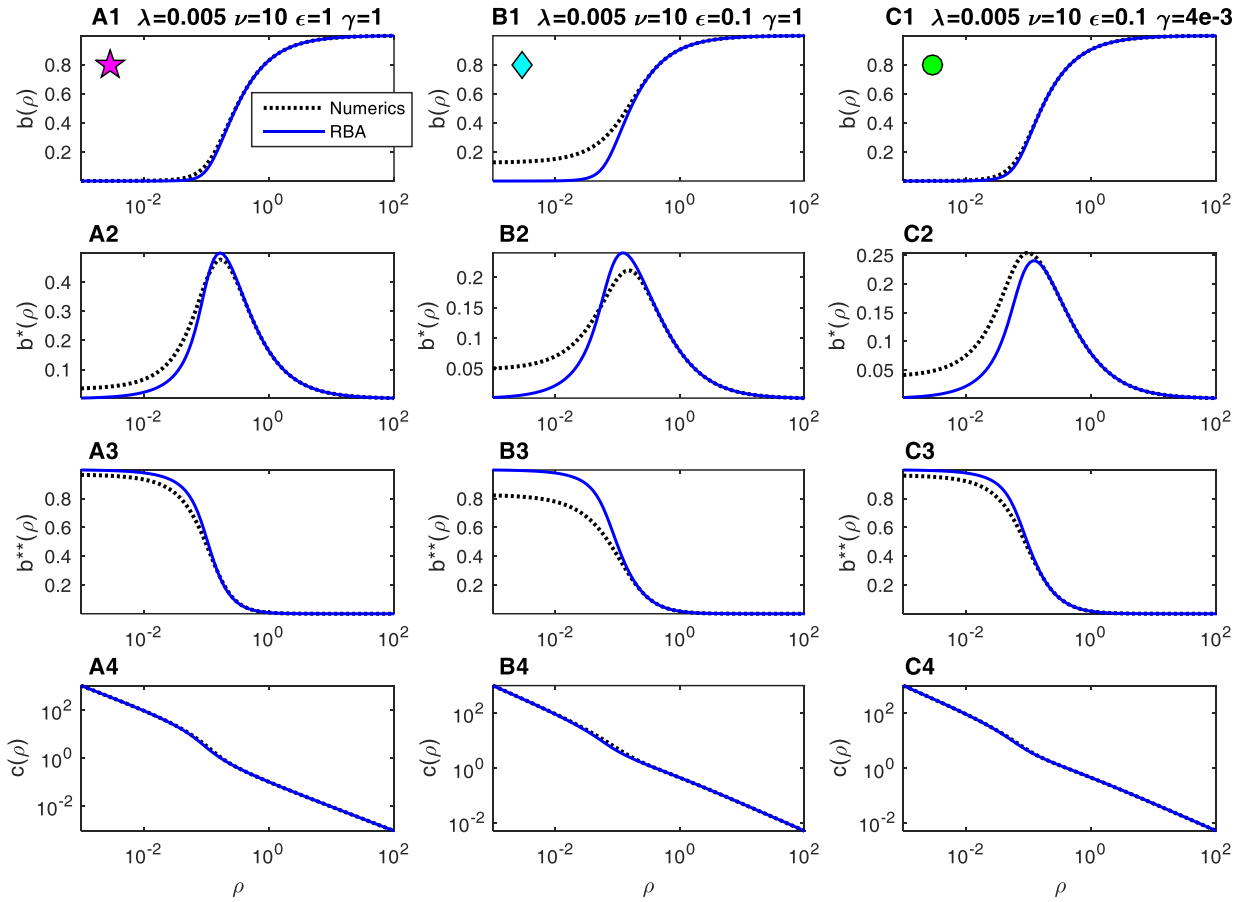

FIGURE 1. Comparison of RBA (solid curves) with numerically computed stationary concentrations (dotted curves), as functions of distance from the Ca^{2+} channel. Each column shows results for a distinct set of non-dimensional cooperativity parameter values labeled at the top. Four rows of panels show respectively the non-dimensional concentrations of free buffer (A1, B1, C1), partially bound buffer (A2, B2, C2), fully bound buffer (A3, B3, C3) and Ca^{2+} (A4, B4, C4). Note that RBA has no dependence on parameters λ and γ. The discrepancy in $[C^{a2+}]$ shown in (A4,B4,C4) is too small to be resolved at this scale, for the given parameter combinations. Symbols in panels (A1,B1,C1) are shown to indicate correspondence with Figs. 2 & 3.

To explore the parameter-dependence hinted by Fig. 1 in more detail, in Fig. 2 the values of λ and ν are systematically varied, for the same three combination of cooperativity parameters (ε, γ) that corresponds to the three columns in Fig. 1. Symbols mark the parameter point (λ=5·10^{-3}, ν=10) corresponding to simulations shown in Fig. 1. The first row of panels, Fig. 2A1-C1, shows the sum of errors in the approximations of *b* and *b*** (error in *b** is excluded since it is uniquely determined from *b* and *b*** by the buffer conservation law), while the second row of panels, Fig. 2A2-C2, shows the discrepancy in the approximation of $[Ca^{2+}]$. We use an absolute deviation measure to quantify the accuracy in buffer approximation, while a logarithmic deviation measure is used to quantify the accuracy in $[Ca^{2+}]$ approximation, in view of the unbounded 1/*ρ* behavior close to the channel source (19, 20):

$$\left\| b_{approx} - b_{numer} \right\| = \frac{1}{N} \sum_{n=1}^{N} \left| b_{approx}(\rho_n) - b_{numer}(\rho_n) \right|, \tag{21}$$

$$\left\| c_{approx} - c_{numer} \right\| = \frac{1}{N} \sum_{n=1}^{N} \left| \log c_{approx}(\rho_n) - \log c_{numer}(\rho_n) \right|. \tag{22}$$

The two deviations measures are computed on a set of N=100 points spanning 5 orders of magnitude of distance ρ, from 10^{-3} to 10^{2}, on a logarithmic scale: $\rho_n = 10^{-3+5n/100}$ (n=1, 2, …, N). The gray shade in Figs. 2 and 3 indicates base-10 logarithm of these deviation measures, with unshaded region corresponding to the average deviation of 10^{-3}, which would be too small to resolve by naked eye. As can be inferred from Figs. 1A1,B1,C1, the error in estimating buffer concentration quantified by Eq. 21 is largely determined by the error in estimating the boundary value of buffer concentration at channel location, $b(0)$.

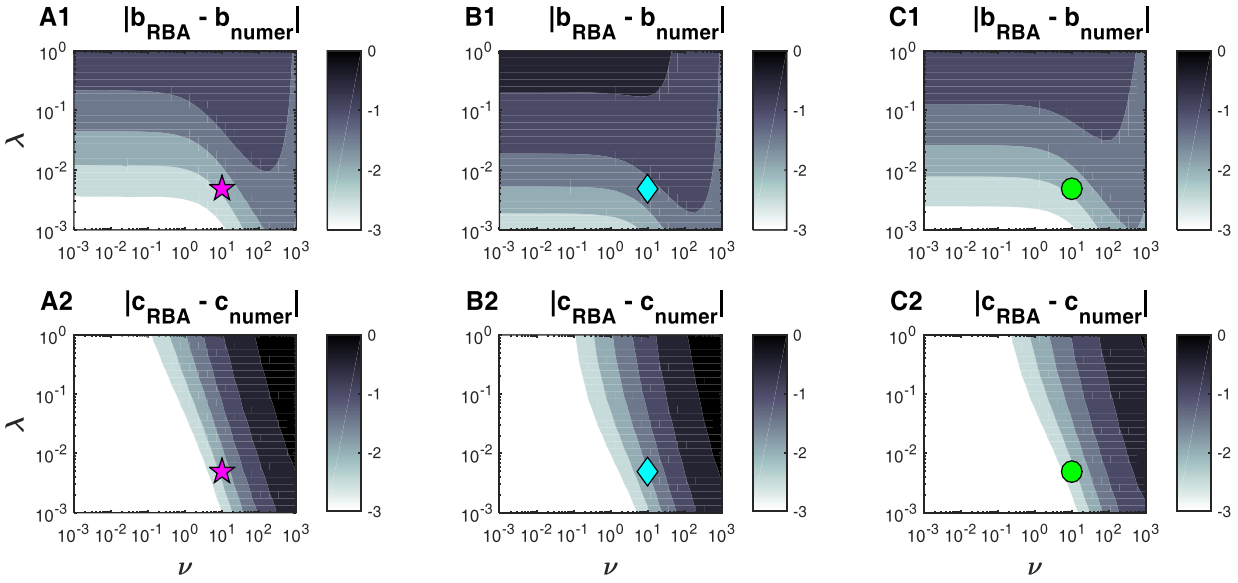

FIGURE 2. RBA accuracy in estimating buffer and Ca^{2+} concentrations, as a function of parameters λ and ν, for the same three values of cooperativity parameters as in Fig. 1: (A1,B1) $\varepsilon = \gamma = 1$; (A2,B2): $\varepsilon = 0.1$, $\gamma = 1$; (A3,B3): $\varepsilon = 0.1$, $\gamma = 4 \cdot 10^{-3}$ (A1,B1,C1): sum of errors in RBA estimates of unbound buffer and fully bound buffer concentrations, according to the error measure given by Eq. 21. (A2,B2,C2): error in RBA estimate of $[Ca^{2+}]$, calculated according to Eq. 22. Symbols mark parameter point corresponding to simulations in Fig. 1*:* λ=0.005, ν=10.

The difference between the two deviation measures given by Eqs. 21, 22 is evident when comparing the rows of panels in Figs. 1 and 2. While the deviation between exact and approximate buffer concentration is the largest near the channel mouth, the relative or logarithmic Ca^{2+} concentration deviation measure is less sensitive to the finite error near the channel, since it is dominated by the free diffusion term $1/\rho$ close to the channel. Therefore, the relative error in $[Ca^{2+}]$ approximation is particularly sensitive to the accuracy of the method at intermediate values of distance, rather than its accuracy in the immediate vicinity of the channel.

To explore the dependence of RBA accuracy on cooperativity parameters ε and γ in more detail, in Fig. 3 we systematically vary the values of these two parameters, given fixed values of λ and ν. These results show in more detail the reduction in RBA accuracy with decreasing ε, and the partial rescue of RBA accuracy by concomitant decrease of cooperativity parameter γ.

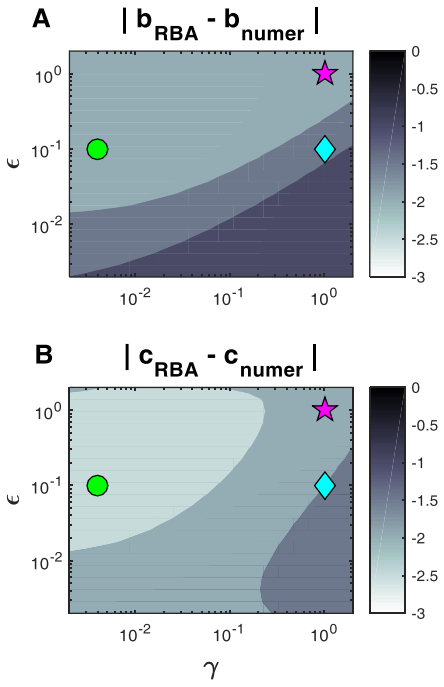

FIGURE 3. RBA accuracy in estimating (A) buffer and (B) Ca^{2+} concentrations, as a function of binding cooperativity parameters ε and γ, for fixed values of RBA parameter λ=5·10^{-3} and buffer strength parameter ν=10 used in Fig. 1. Deviation measures are the same as in Fig. 2. Symbols mark the three parameter points corresponding to the three panel columns in Figs 1 & 2*: asterisks*: $\varepsilon = \gamma = 1$; *diamonds*: $\varepsilon = 0.1$, $\gamma = 1$; *circles*: $\varepsilon = 0.1$, $\gamma = 4 \cdot 10^{-3}$.

Figures 1-3 show that the main challenge in the application of RBA to biological two-site buffers is their high degree of cooperativity. In order to evaluate whether RBA is applicable to such high values of Ca^{2+} binding cooperativity, in Figure 4 we simulate the Ca^{2+} nanodomain in the presence of 100μM of Ca^{2+} buffer with the properties of either calretinin or one of the two lobes of calmodulin, which all have extreme cooperativity values of $\varepsilon < 10^{-2}$ (36, 40). In agreement with the parameter dependence discussed above, RBA achieves reasonable accuracy only for the N-lobe of calmodulin, since it's the only one of the three buffers with a moderately low value of 2nd cooperativity parameter: γ = 0.4. For this buffer, the accuracy of RBA is quite good for the considered Ca^{2+} current amplitude of I_{Ca}=0.4pA and total buffer concentration B_T=100μM, which correspond to values λ =1.8·10^{-4} and ν =25.4, within ranges favorable to the RBA regime.

We note that the good performance of RBA for the N-lobe of calmodulin is of interest, despite the poor performance of RBA for the C-lobe, since C-lobe has significantly slower Ca^{2+} binding rate, and would not influence the nanodomain on short time scales. In fact, previous modeling studies show an interesting effect of Ca^{2+} hand-over from the N-lobe to the C-lobe upon the termination of the Ca^{2+} influx (41). Thus, the contribution of the C-lobe to Ca^{2+} binding mostly occurs after the termination of the Ca^{2+} influx, and the full Ca^{2+} binding dynamics would reveal multiple time scales.

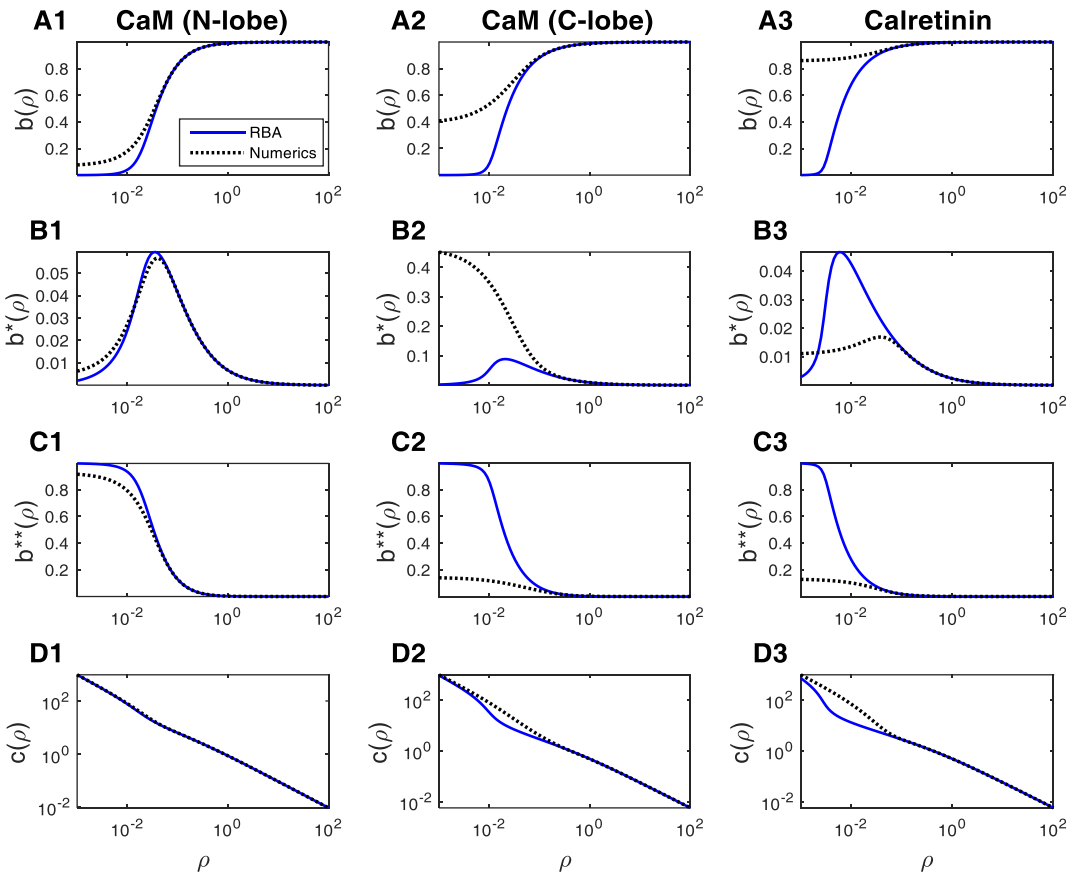

FIGURE 4. Comparison of RBA with numerical simulations of a single-channel Ca^{2+} nanodomain with current I_{Ca}=0.4 pA, in the presence of 100 μM buffer with Ca^{2+}-binding properties similar to: (A1-D1) N-lobe of calmodulin; (A2-D2) C-lobe of calmodulin; (A3-D3) calretinin. From top to bottom, panels show (A1-A3) free buffer, (B1-B3) partially bound buffer, (C1-C3) fully bound buffer, and (D1-D3) Ca^{2+} concentration. Buffer parameters are listed in Table 1.

Buffering capacity and time-dependent RBA

Finally, we examine buffering capacity of a two-to-one buffer, which is an informative characteristic naturally emerging from the RBA assumptions already in a single-compartment, non-spatial model of Ca^{2+} influx and buffering (14, 47, 48). Buffering capacity equals the marginal increase in buffer-bound Ca^{2+} relative to free Ca^{2+}, and therefore quantifies the fraction of Ca^{2+} ions that become bound to the buffer. In most cells, resting buffering capacity (capacity at background Ca^{2+} concentration) is found to lie in the range from 20 to 2000, indicating that 80% to 99.95% of Ca^{2+} influx is buffer-bound soon upon its entry into the cytoplasm (6, 7, 49). For a cooperative buffer, buffering capacity was first considered by (39), and is obtained by differentiating bound [Ca^{2+}], expressed by Eqs. 13, with respect to free [Ca^{2+}]:

$$\kappa \equiv \frac{d\left(B^{*}+2B^{**}\right)}{dC} = 2B_T K_2 \frac{K_1K_2 + C\left[2K_1 + C\right]}{\left[K_1K_2 + C\left(2\,K_2 + C\right)\right]^2} \tag{23}$$

In deriving this result, we set $\delta_B^{*} = \delta_B^{**} = 1$, since the standard definition of buffering capacity does not retain its simple meaning when buffer mobility is affected by Ca^{2+} binding. In non-dimensional variables, Eq. 23 becomes

$$\kappa = \frac{2B_T}{K_1}\frac{1+c\left[2+\varepsilon c\right]}{\left[1+\varepsilon c\ (2+c)\right]^2} \tag{24}$$

At rest ([Ca^{2+}]≈0), this expression gives an intuitive result $\kappa(0) = 2B_T / K_1$, equivalent to the resting capacity of a simple buffer of affinity K_1 and concentration $2B_T$, given two binding sites per molecule. As explored in (36, 39), the cooperative nature of buffering is reflected in the fact that buffer capacity is a non-monotonic function of [Ca^{2+}] when $\varepsilon < 1$: it increases with [Ca^{2+}] for small concentrations, but eventually decreases due to buffer saturation as Ca^{2+} concentration is increased further, as shown in Fig. 5. As compared to a cooperative buffer, buffering capacity of a non-cooperative buffer is always decreasing: setting $\varepsilon = 1$, and factorizing the numerator and denominator in Eq. 24, one obtains a familiar expression $\kappa = 2B_T / \left[K\ (1+c)^2\right]$, where $K = k^- / k^+$ is the non-cooperative dissociation constant, and c = [Ca^{2+}] / K (47).

Figure 5 shows that for cooperative buffers listed in Table 1, buffering capacity achieves its maximum within physiological, micromolar range of local intracellular Ca^{2+} signals, suggesting that this property of cooperative buffering is indeed likely to have physiological relevance (36, 39). Figure 5 also compares the capacity of each cooperative buffer to that of a non-cooperative buffer with an effective affinity given by the geometric mean of the affinities of the two binding steps of a cooperative buffer (36).

Finally, the concept of buffering capacity allows one to obtain a time-dependent RBA, which assumes that the reaction is always at equilibrium, but concentrations are varying in time. Following prior work (26-29), we assume that buffer mobility is not affected by Ca^{2+} binding, $\delta_B^* = \delta_B^{**} = 1$. In this case the derivation of time-dependent RBA is completely analogous to the case of a simple buffer, and is obtained by applying the chain rule to the Ca^{2+} conservation condition, Eq. 5, expressing derivatives of bound Ca^{2+} in terms of the corresponding derivatives of free [Ca^{2+}]. This reduces the dimensionality of the problem down to a single equation for the free [Ca^{2+}]. Introducing non-dimensional space and time, $\rho \equiv r / L$ and $\tau = t\ D_C / L^2$, where length-scale L is given by Eq. 10, one obtains:

$$\partial_\tau c = \frac{1+\kappa D}{1+\kappa}\ \nabla_\rho^2 c + \frac{D}{1+\kappa}\frac{d\kappa}{dc}\left|\nabla_\rho c\right|^2 \tag{25}$$

where $D \equiv D_B / D_C$. Satisfyingly, this equation has the same form as the time-dependent RBA for a non-cooperative buffer (19, 26-29), except for the different functional form of the buffering capacity, given by Eq. 24. Although this equation is not analytically solvable, it provides a qualitative description of effective Ca^{2+} diffusion coefficient as a non-linear function of [Ca^{2+}] and buffer properties (26-28, 48). We note that it is possible to generalize this derivation to the case where buffer mobility is changed by Ca^{2+} binding. However, in this case the resulting expressions are too complicated to be of practical use, even in the case of a simple buffer (see Appendix in (26)).

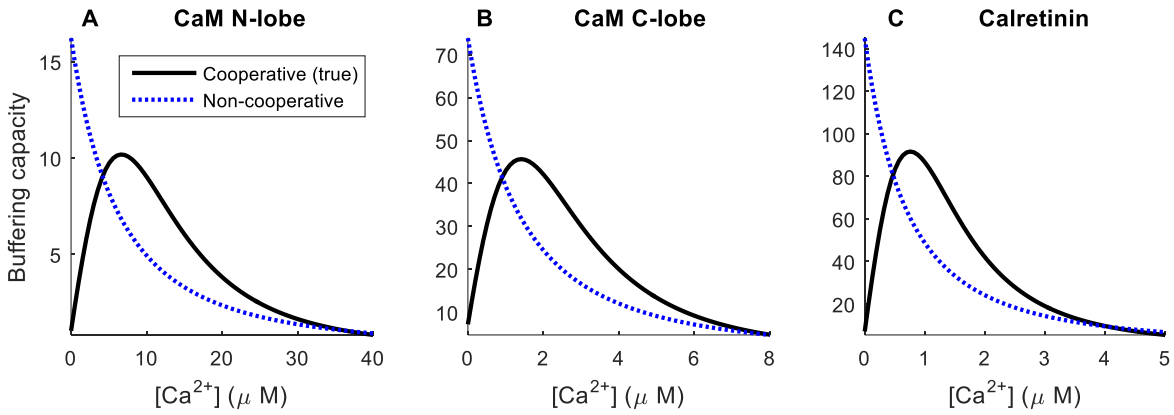

FIGURE 5. Non-monotonic dependence of buffering capacity (Eq. 23) on Ca^{2+} concentration for cooperative two-to-one buffers listed in Table 1: (A) N-lobe of calmodulin, (B) C-lobe of calmodulin, and (C) calretinin. Solid curves show the actual cooperative buffer capacity given by Eq. 23, while the dotted curves show for comparison the capacity of a non-cooperative buffer of the same binding site concentration (200μM), but with an effective affinity given by the geometric average of the two binding site affinities, $K = \sqrt{K_1 K_2}$ (36)

DISCUSSION

As demonstrated by early modeling studies, quasi-stationary Ca^{2+} concentration domains are established within microseconds upon the opening of a single channel, and collapse as rapidly after the channels close (10-13, 50). Therefore, RBA and other closed-form approximations of stationary single-channel nanodomains may provide sufficient accuracy in estimating Ca^{2+} and buffer concentration near an open Ca^{2+} channel. Further, their use is not limited to describing static single-channel nanodomains, but also allows approximating Ca^{2+} concentration near an array of Ca^{2+} channels with time-dependent gating. In this case the channel opening events are simulated independently, while the Ca^{2+} domains are assumed to establish instantly near each open channel and are computed using static approximations such as RBA. This provides a computational efficient hybrid approach to modeling cell Ca^{2+} dynamics (22) (see also (51)). Parenthetically, we note however that the accuracy of any approach based on deterministic solutions to Ca^{2+} dynamics was found to be reduced if Ca^{2+} channel gating is Ca^{2+}-dependent (as for inositol-3-phosphate and ryanodine receptor-coupled Ca^{2+} channels), since in this case stochastic Ca^{2+} fluctuations have a greater importance and cannot be neglected (51, 52), with the size of fluctuations further increased by Ca^{2+} buffering (53).

As expected, the parameter regions where RBA is accurate is reduced for highly cooperative buffers. This loss of accuracy is more apparent if the Ca^{2+} binding cooperativity is caused by the increases in the forward binding rate, as for calretinin and C-lobe of calmodulin (Fig. 4). If on the other hand cooperativity is caused by the decrease in the unbinding rate of the second reaction ($\gamma << 1$), RBA accuracy is similar to that for non-cooperative buffer. This result is intuitive, since for $\varepsilon << 1$, $\gamma = O(1)$, the rate of the first Ca^{2+} binding reaction would be small, invalidating the RBA assumption that Ca^{2+} binding is fast compared to the rate of Ca^{2+} diffusion.

Figs. 1-4 demonstrate that RBA can achieve sufficient accuracy even in the case of some (but not all) highly cooperative buffers. Here it should be noted that the properties of many buffers are still not fully characterized. A widely expressed class of buffers and sensors phylogenetically close to calmodulin include neuronal Ca^{2+}

sensor proteins (NCS), calhedrin, hippocalcin, and many others (38), some of which may have more moderate values of Ca^{2+}-binding cooperativity.

Our ultimate goal is to contribute to the extension of previously developed modeling methods and results to more realistic buffers, including cooperative buffers. Cooperative Ca^{2+} binding is likely to play important, yet unexplored roles in shaping cell Ca^{2+} signals in a highly non-trivial way. Apart from affecting the dynamics of biochemical interactions downstream of Ca^{2+} binding, recent results indicate that cooperative buffering may have a more immediate effect on Ca^{2+} dynamics. For example, it has been shown that cooperative buffers decrease the facilitation of Ca^{2+} transients associated with buffers saturation (34, 39), but may increase short-term synaptic facilitation through a different mechanism of buffer dislocation (54). Further, as noted above, the very ability of cooperative buffers to absorb Ca^{2+} depends in a highly non-trivial way on the background Ca^{2+} concentration (Fig. 5). Computational modeling of calmodulin Ca^{2+} binding and downstream biochemical interactions is a subject of intense recent work, and is indispensable for the understanding of long-term synaptic plasticity and other fundamental physiological processes (37-41, 55-57). Better description of Ca^{2+} dynamics in the presence of cooperative buffers may also be of use for accurate interpretation of optogenetic measurements with genetically-encoded fluorescent Ca^{2+} dyes, which are formed by fusing a calmodulin molecule with a green fluorescent protein (58-63).

RBA is quite likely not the only approximation that can be applied to complex Ca^{2+} buffers. For example, we are currently exploring approximation methods based on matching short- and long-range asymptotic expansions of single-channel nanodomains, analogous to the Padė approximations method that we recently developed for simple buffers (20). Such approximations may have more uniform error dependence on buffering parameters.

ACKNOWLEDGEMENTS

This work was supported by the National Science Foundation grant DMS-1517085.

APPENDIX: RBA with non-zero Ca^{2+} at infinity

Here we consider the case of non-zero [Ca^{2+}] far from the channel, but for the sake of clarity restrict to the case of binding-independent buffer diffusivity: $D_B = D_B^* = D_B^{**}$ ($\delta_B^* = \delta_B^{**} = 1$). In this case the RBA derivation is qualitatively similar to the one considered in Results, but the integration of conservation laws leads to an extra boundary term describing the non-trivial condition at infinity. Namely, Eqs. 7-8 are modified as follows:

$$B + B^* + B^{**} = B_\infty + B_\infty^* + B_\infty^{**} \equiv B_T\,, \tag{26}$$

$$D_C C + D_B\left(B^* + 2B^{**}\right) = \frac{1}{2\pi z F}\sum_{k=1}^{N}\frac{I_k^{Ca}}{|r - r_k|} + D_C C_\infty + D_B\left(B_\infty^* + 2B_\infty^{**}\right). \tag{27}$$

Here C_∞, B_∞, B_∞^* and B_∞^{**} describe Ca^{2+} and buffer concentrations infinitely far from the channel. These four quantities are not independent, but are related by the point-wise reaction equilibrium conditions given by Eq. 13, with $\delta_B^* = \delta_B^{**} = 1$. Eq. 27 then leads to the following generalization of the RBA condition given by Eq. 14

$$C\left[D_C + \frac{2D_B B_T\left(K_2 + C\right)}{K_1 K_2 + C\left(2K_2 + C\right)}\right] = \frac{1}{4\pi F}\sum_{k=1}^{N}\frac{I_k^{Ca}}{|r - r_k|} + X_\infty\,. \tag{28}$$

X_∞ denotes the boundary value of the linear combination on the left-hand side of Eqs. 27, 28, taken infinitely far from the channel:

$$\begin{aligned} X_\infty &= D_C C_\infty + D_B\left(B_\infty^* + 2B_\infty^{**}\right) \\ &= C_\infty\left[D_C + \frac{2D_B B_T\left(K_2 + C_\infty\right)}{K_1 K_2 + C_\infty\left(2K_2 + C_\infty\right)}\right]. \end{aligned} \tag{29}$$

In non-dimensional form, buffer concentrations are normalized by B_T; considering the case of a single channel only, the RBA equation accepts the form

$$c\left[1 + \frac{\nu\varepsilon\left(1 + c\right)}{1 + \varepsilon c\left(2 + c\right)}\right] = \frac{1}{\rho} + x_\infty\,, \tag{30}$$

$$\text{where } x_\infty = c_\infty\left[1 + \frac{\nu\varepsilon\left(1 + c_\infty\right)}{1 + \varepsilon c_\infty\left(2 + c_\infty\right)}\right].$$

This solution to this equation is very similar to the solution of Eq. 17, and is given by Eqs. 18-19, but with the following re-definitions of functions *U*, *F* and *G*:

$$\begin{cases} U = F\left(F^2 - \dfrac{3G}{2}\right) + \dfrac{1 + x_\infty\rho}{2\varepsilon\rho}\,, \\ F = \dfrac{1 - \rho\left(2 + \nu - x_\infty\right)}{3\rho}\,, \\ G = \dfrac{\rho\left(1 + \varepsilon\left(\nu - 2x_\infty\right)\right) - 2\varepsilon}{3\varepsilon\rho}\,. \end{cases} \tag{31}$$

REFERENCES

1. Konieczny, V., M. V. Keebler, and C. W. Taylor. 2012. Spatial organization of intracellular Ca2+ signals. Semin Cell Dev Biol 23:172-180.
2. Oheim, M., F. Kirchhoff, and W. Stuhmer. 2006. Calcium microdomains in regulated exocytosis. Cell Calcium 40:423-439.
3. Berridge, M. J., P. Lipp, and M. D. Bootman. 2000. The versatility and universality of calcium signalling. Nat Rev Mol Cell Biol 1:11-21.
4. Augustine, G. J., F. Santamaria, and K. Tanaka. 2003. Local calcium signaling in neurons. Neuron 40:331-346.
5. Stanley, E. F. 2016. The Nanophysiology of Fast Transmitter Release. Trends Neurosci 39:183-197.
6. Matthews, E. A., and D. Dietrich. 2015. Buffer mobility and the regulation of neuronal calcium domains. Front Cell Neurosci 9:48.
7. Neher, E. 2000. Calcium buffers in flash-light. Biophys J 79:2783-2784.
8. Cheng, H., and W. J. Lederer. 2008. Calcium sparks. Physiol Rev 88:1491-1545.
9. Thurley, K., A. Skupin, R. Thul, and M. Falcke. 2012. Fundamental properties of Ca2+ signals. Biochim Biophys Acta 1820:1185-1194.
10. Roberts, W. M. 1993. Spatial calcium buffering in saccular hair cells. Nature 363:74-76.
11. Simon, S. M., and R. R. Llinas. 1985. Compartmentalization of the submembrane calcium activity during calcium influx and its significance in transmitter release. Biophy. J. 48:485-498.
12. Fogelson, A. L., and R. S. Zucker. 1985. Presynaptic calcium diffusion from various arrays of single channels. Implications for transmitter release and synaptic facilitation. Biophys. J. 48:1003-1017.
13. Chad, J. E., and R. Eckert. 1984. Calcium domains associated with individual channels can account for anomalous voltage relations of CA-dependent responses. Biophys J 45:993-999.
14. Neher, E. 1998. Usefulness and limitations of linear approximations to the understanding of Ca++ signals. Cell Calcium 24:345-357.
15. Dupont, G., M. Falcke, V. Kirk, and J. Sneyd. 2016. Models of Calcium Signalling. Springer.
16. Aharon, S., H. Parnas, and I. Parnas. 1994. The magnitude and significance of Ca2+ domains for release of neurotransmitter. Bull Math Biol 56:1095-1119.
17. Sala, F., and A. Hernandez-Cruz. 1990. Calcium diffusion modeling in a spherical neuron. Relevance of buffering properties. Biophys J 57:313-324.
18. Nowycky, M. C., and M. J. Pinter. 1993. Time courses of calcium and calcium-bound buffers following calcium influx in a model cell. Biophys J 64:77-91.
19. Smith, G. D., L. X. Dai, R. M. Miura, and A. Sherman. 2001. Asymptotic analysis of buffered calcium diffusion near a point source. Siam J Appl Math 61:1816-1838.
20. Matveev, V. 2016. Pade Approximation of a Stationary Single-Channel Ca2+ Nanodomain. Biophys J 111:2062-2074.

21. Coggins, M., and D. Zenisek. 2009. Evidence that exocytosis is driven by calcium entry through multiple calcium channels in goldfish retinal bipolar cells. J Neurophysiol 101:2601-2619.

22. Nguyen, V., R. Mathias, and G. D. Smith. 2005. A stochastic automata network descriptor for Markov chain models of instantaneously coupled intracellular Ca2+ channels. Bull Math Biol 67:393-432.

23. Bertram, R., G. D. Smith, and A. Sherman. 1999. Modeling study of the effects of overlapping Ca2+ microdomains on neurotransmitter release. Biophys J 76:735-750.

24. Trommershauser, J., R. Schneggenburger, A. Zippelius, and E. Neher. 2003. Heterogeneous presynaptic release probabilities: functional relevance for short-term plasticity. Biophys J 84:1563-1579.

25. Pape, P. C., D. S. Jong, and W. K. Chandler. 1995. Calcium release and its voltage dependence in frog cut muscle fibers equilibrated with 20 mM EGTA. J Gen Physiol 106:259-336.

26. Wagner, J., and J. Keizer. 1994. Effects of rapid buffers on Ca2+ diffusion and Ca2+ oscillations. Biophys J 67:447-456.

27. Smith, G. D., J. Wagner, and J. Keizer. 1996. Validity of the rapid buffering approximation near a point source of calcium ions. Biophys J 70:2527-2539.

28. Smith, G. D. 1996. Analytical steady-state solution to the rapid buffering approximation near an open Ca2+ channel. Biophys J 71:3064-3072.

29. Sneyd, J., Dale, P.D., and A. Duffy. 1998. Traveling waves in buffered systems: applications to calcium waves. Siam J Appl Math 58:1178-1192.

30. Stern, M. D. 1992. Buffering of calcium in the vicinity of a channel pore. Cell Calcium 13:183-192.

31. Naraghi, M., and E. Neher. 1997. Linearized buffered Ca2+ diffusion in microdomains and its implications for calculation of [Ca2+] at the mouth of a calcium channel. J Neurosci 17:6961-6973.

32. Bentele, K., and M. Falcke. 2007. Quasi-steady approximation for ion channel currents. Biophys J 93:2597-2608.

33. Neher, E. 1998. Vesicle pools and Ca2+ microdomains: new tools for understanding their roles in neurotransmitter release. Neuron 20:389-399.

34. Schwaller, B. 2009. The continuing disappearance of "pure" Ca2+ buffers. Cell Mol Life Sci 66:275-300.

35. Schwaller, B. 2014. Calretinin: from a "simple" Ca(2+) buffer to a multifunctional protein implicated in many biological processes. Front Neuroanat 8:3.

36. Faas, G. C., B. Schwaller, J. L. Vergara, and I. Mody. 2007. Resolving the fast kinetics of cooperative binding: Ca2+ buffering by calretinin. PLoS Biol 5:e311.

37. Chin, D., and A. R. Means. 2000. Calmodulin: a prototypical calcium sensor. Trends Cell Biol 10:322-328.

38. Raghuram, V., Y. Sharma, and M. R. Kreutz. 2012. Ca(2+) sensor proteins in dendritic spines: a race for Ca(2+). Front Mol Neurosci 5:61.

39. Saftenku, E. E. 2012. Effects of Calretinin on Ca(2+) Signals in Cerebellar Granule Cells: Implications of Cooperative Ca(2+) Binding. Cerebellum 11:102-120.

40. Faas, G. C., S. Raghavachari, J. E. Lisman, and I. Mody. 2011. Calmodulin as a direct detector of Ca2+ signals. Nat Neurosci 14:301-304.

41. Kubota, Y., and M. N. Waxham. 2010. Lobe specific Ca2+-calmodulin nano-domain in neuronal spines: a single molecule level analysis. PLoS Comput Biol 6:e1000987.

42. Falcke, M. 2003. On the role of stochastic channel behavior in intracellular Ca2+ dynamics. Biophys J 84:42-56.

43. Falcke, M. 2003. Buffers and oscillations in intracellular Ca2+ dynamics. Biophys J 84:28-41.

44. Thul, R., and M. Falcke. 2004. Release currents of IP(3) receptor channel clusters and concentration profiles. Biophys J 86:2660-2673.

45. Matveev, V. 2016. CalC (Calcium Calculator) simulation software, release version 7.8.6. V. Matveev, editor.

46. Matveev, V., A. Sherman, and R. S. Zucker. 2002. New and corrected simulations of synaptic facilitation. Biophys J 83:1368-1373.

47. Neher, E., and G. J. Augustine. 1992. Calcium gradients and buffers in bovine chromaffin cells. J Physiol 450:273-301.

48. Irving, M., J. Maylie, N. L. Sizto, and W. K. Chandler. 1990. Intracellular diffusion in the presence of mobile buffers. Application to proton movement in muscle. Biophys J 57:717-721.

49. Delvendahl, I., L. Jablonski, C. Baade, V. Matveev, E. Neher, and S. Hallermann. 2015. Reduced endogenous Ca2+ buffering speeds active zone Ca2+ signaling. Proc Natl Acad Sci U S A 112:E3075-3084.

50. Zucker, R. S., and A. L. Fogelson. 1986. Relationship between transmitter release and presynaptic calcium influx when calcium enters through discrete channels. Proc Natl Acad Sci U S A 83:3032-3036.

51. Rudiger, S., J. W. Shuai, W. Huisinga, C. Nagaiah, G. Warnecke, I. Parker, and M. Falcke. 2007. Hybrid stochastic and deterministic simulations of calcium blips. Biophys J 93:1847-1857.

52. Wieder, N., R. Fink, and F. von Wegner. 2015. Exact stochastic simulation of a calcium microdomain reveals the impact of Ca(2)(+) fluctuations on IP(3)R gating. Biophys J 108:557-567.

53. Weinberg, S. H., and G. D. Smith. 2014. The influence of Ca(2)(+) buffers on free [Ca(2)(+)] fluctuations and the effective volume of Ca(2)(+) microdomains. Biophys J 106:2693-2709.

54. Timofeeva, Y., and K. E. Volynski. 2015. Calmodulin as a major calcium buffer shaping vesicular release and short-term synaptic plasticity: facilitation through buffer dislocation. Front Cell Neurosci 9:239.

55. Keller, D. X., K. M. Franks, T. M. Bartol, Jr., and T. J. Sejnowski. 2008. Calmodulin activation by calcium transients in the postsynaptic density of dendritic spines. PLoS One 3:e2045.

56. Griffith, T., K. Tsaneva-Atanasova, and J. R. Mellor. 2016. Control of Ca2+ Influx and Calmodulin Activation by SK-Channels in Dendritic Spines. PLoS Comput Biol 12:e1004949.

57. Dick, I. E., M. R. Tadross, H. Liang, L. H. Tay, W. Yang, and D. T. Yue. 2008. A modular switch for spatial Ca2+ selectivity in the calmodulin regulation of CaV channels. Nature 451:830-834.

58. Tallini, Y. N., M. Ohkura, B. R. Choi, G. Ji, K. Imoto, R. Doran, J. Lee, P. Plan, J. Wilson, H. B. Xin, A. Sanbe, J. Gulick, J. Mathai, J. Robbins, G. Salama, J. Nakai, and M. I. Kotlikoff. 2006. Imaging cellular signals in the heart in vivo: Cardiac expression of the high-signal Ca2+ indicator GCaMP2. Proc Natl Acad Sci U S A 103:4753-4758.

59. Tian, L., S. A. Hires, T. Mao, D. Huber, M. E. Chiappe, S. H. Chalasani, L. Petreanu, J. Akerboom, S. A. McKinney, E. R. Schreiter, C. I. Bargmann, V. Jayaraman, K. Svoboda, and L. L. Looger. 2009. Imaging neural activity in worms, flies and mice with improved GCaMP calcium indicators. Nat Methods 6:875-881.

60. Wilms, C. D., and M. Hausser. 2009. Lighting up neural networks using a new generation of genetically encoded calcium sensors. Nat Methods 6:871-872.

61. Dreosti, E., B. Odermatt, M. M. Dorostkar, and L. Lagnado. 2009. A genetically encoded reporter of synaptic activity in vivo. Nat Methods 6:883-889.

62. Chen, T. W., T. J. Wardill, Y. Sun, S. R. Pulver, S. L. Renninger, A. Baohan, E. R. Schreiter, R. A. Kerr, M. B. Orger, V. Jayaraman, L. L. Looger, K. Svoboda, and D. S. Kim. 2013. Ultrasensitive fluorescent proteins for imaging neuronal activity. Nature 499:295-300.

63. Nakai, J., M. Ohkura, and K. Imoto. 2001. A high signal-to-noise Ca(2+) probe composed of a single green fluorescent protein. Nat Biotechnol 19:137-141.